

Metamagnetic transitions and anomalous magnetoresistance in EuAg_4As_2 crystal

Qinqing Zhu,^{1,*} Liang Li,^{1,*} Zhihua Yang,¹ Zhefeng Lou,² Jianhua Du,³
Jinhu Yang,¹ Bin Chen,¹ Hangdong Wang,^{1,†} and Minghu Fang^{2,4,‡}

¹*Hangzhou Key Laboratory of Quantum Matter, Department of Physics,
Hangzhou Normal University, Hangzhou 311121, China*

²*Department of Physics, Zhejiang University, Hangzhou 310027, China*

³*Department of Physics, China Jiliang University, Hangzhou 310018, China*

⁴*Collaborative Innovation Center of Advanced Microstructures, Nanjing University, Nanjing 210093, China*
(Dated: January 25, 2022)

In this paper, the magnetic and transport properties were systematically studied for EuAg_4As_2 single crystals, crystallizing in a centrosymmetric trigonal CaCu_4P_2 type structure. It was found that two magnetic transitions occur at $T_{N1} = 10$ K and $T_{N2} = 15$ K, respectively, which are driven to lower temperatures by applied magnetic field. Below T_{N1} , two successive metamagnetic transitions were observed when a magnetic field is applied in the ab plane ($H \parallel ab$ plane). For both $H \parallel ab$ and $H \parallel c$, EuAg_4As_2 shows a positive, unexpected large magnetoresistance (up to 202%) at low fields below T_{N1} , and a large negative magnetoresistance (up to -78%) at high fields/intermediate temperatures, which may have potential application in the magnetic sensors. Finally, the magnetic phase diagrams of EuAg_4As_2 were constructed for both $H \parallel ab$ and $H \parallel c$ by using the resistivity and magnetization data.

PACS numbers: 75.47.-m, 75.30.Kz

Keywords: anomalous magnetoresistance; metamagnetic transition; magnetic phase diagram

I. INTRODUCTION

Responses of Eu-based compounds to external fields have generated immense interest due to exhibiting many exotic properties, such as valence transition¹, Kondo behavior², quantum hall effect³, novel magnetoresistance (MR)^{4,5}, resulted from their complicated, tunable magnetic ground states with large local moments. In those modulated systems with an incommensurate magnetic structure induced by the strong competing interactions involving the magnetic moments, the lattice, and/or the conduction electrons, like the long-range Ruderman-Kittel-Kasuya-Yosida (RKKY) type coupling, one or several successive transitions have been observed at low temperatures when a magnetic field is applied, leading to complex magnetic phase diagrams⁶.

The Eu-based ternary pnictide EuAg_4As_2 , crystallizing in a centrosymmetric trigonal CaCu_4P_2 type structure (space group $R\bar{3}m$, No. 166), was first reported by Stoyko *et al.*⁷. The structure can be considered as the derivative from the trigonal CaAl_2Si_2 -type structure, by inserting an additional itinerant Ag_2 layer between the close-packed Ag_2As_2 layers. Unlike in CaCu_4P_2 , where the Cu2 sites are fully occupied, the Ag2 sites are split into three isotropic and equally partially occupied sites in EuAg_4As_2 [see Fig. 1(b)]. To the authors' knowledge, a few studies on the physical properties of the ternary CaCu_4P_2 type pnictides AAg_4Pn_2 ($A = \text{Sr}, \text{Eu}$; $\text{Pn} = \text{As}, \text{Sb}$) have been reported. For SrAg_4As_2 , the quantum oscillation measurements reveal small Fermi pockets with light effective masses and unexpected high mobilities, in contrast with the predication of the first-principle calculations⁸. For the magnetic EuAg_4As_2 , based on the measurements of magnetization⁹, neutron diffraction¹⁰,

¹⁵¹Eu Mössbauer spectroscopy^{9,11} and pressure effects¹², it was found that a structural distortion occurs at about 120 K, and two magnetic transitions emerge at 15 K and 9K, respectively, below 9 K, an incommensurate, non-collinear long-range antiferromagnetic (AFM) state; between 9 - 15 K, a long-range magnetic order with the $\text{Eu}^{2+} 4f^7$ spin moments having an incommensurate sine modulated structure. However, there are no reports about the magnetotransports and the phase diagram for this low-dimensional system with so rich magnetic structures.

In this article, we report the magnetization and MR measurements on EuAg_4As_2 single crystal. It is confirmed that two magnetic transitions occur at $T_{N1} = 10$ K and $T_{N2} = 15$ K, respectively, with the magnetic moments almost lying in the ab plane. We further observed that the magnetic transition temperatures, T_{N1} and T_{N2} , decrease with increasing magnetic field and two successive metamagnetic (MM) transitions occurring at 0.5 T and 0.95 T field applied in the ab plane at 2 K. Interestingly, it was found that an anomalous MR emerges for both $H \parallel ab$ and $H \parallel c$ orientations, with different magnetic field dependence at various temperature range, which is related to the magnetic ground states. Finally, we constructed the phase diagrams based on the data of the magnetization and resistivity measurements.

II. EXPERIMENTAL METHODS

EuAg_4As_2 crystals were grown using a self-flux method. First, Eu chunks, and Ag, As powders were mixed with a ratio of 1:4:2 and were put into an alumina crucible and sealed in an evacuated silica tube. The mix-

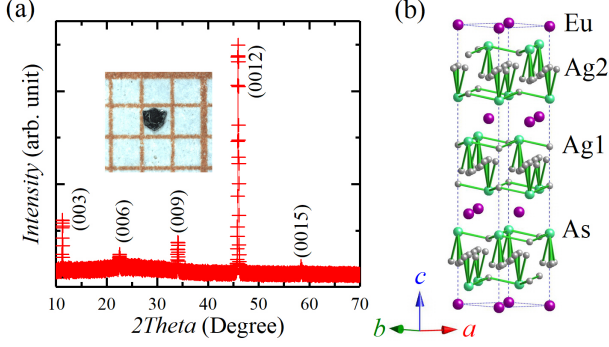


FIG. 1. (Color online) (a) Single crystal XRD pattern of EuAg_4As_2 . Inset: A photograph of a EuAg_4As_2 single crystal. (b) Crystal structure of EuAg_4As_2 . Europium, silver, and arsenic atoms are drawn as purple, grey, and green spheres, respectively.

TABLE I. The fitting parameters of the high temperature susceptibility for EuAg_4As_2 single crystal.

Parameters	$H \parallel c$ axis	$H \parallel ab$ plane
χ_0 (emu/mol)	0.03578	-0.00228
C (emu·K/mol)	7.88	7.91
θ (K)	10.3	14.1
μ_{eff} (μ_B/Eu)	7.94	7.95

ture was heated up to 1100 °C and kept for 24 hours, then cooled down to 700 °C at a rate of 3 °C/h. Finally the furnace was cooled to room temperature after shutting down the power. Single crystals with a typical dimension of $0.8 \times 0.8 \times 0.2 \text{ mm}^3$ [see the inset of Fig. 1(a)], were mechanically exfoliated from the flux. The crystal composition was determined by the Energy-dispersive X-ray spectroscopy (EDX) in a Zeiss Supra 55 scanning electron microscope to be the stoichiometric EuAg_4As_2 . The crystal structure was confirmed by X-ray diffraction (XRD) performed at room temperature on a Rigaku X-ray diffractometer with $\text{Cu } K\alpha_1$ radiation [see Fig. 1(a)]. All XRD peaks are indexed to be $(00l)$ planes, and the cell parameter c is yielded to be about 23.65 Å, in consistent with the previous result¹⁰. The magnetization was measured using the *Quantum Design* Magnetic Properties Measurement System (MPMS-VSM-7T). The resistivity measurements were carried out by the standard four-probe technique on the *Quantum Design* Physical Properties Measurement System (PPMS-9T).

III. RESULTS AND DISCUSSIONS

Figure 2 shows the temperature dependence of magnetic susceptibility, χ_{ab} ($H \parallel ab$ plane) and χ_c ($H \parallel c$ axis), respectively, measured at magnetic field of 1 kOe with a zero field cooling (ZFC) process for a EuAg_4As_2 crystal. The higher temperature ($> 50 \text{ K}$) $\chi_{ab}(T)$ data can be well fitted by the Curie-Weiss law, $\chi = \chi_0 + \frac{C}{T - \theta}$,

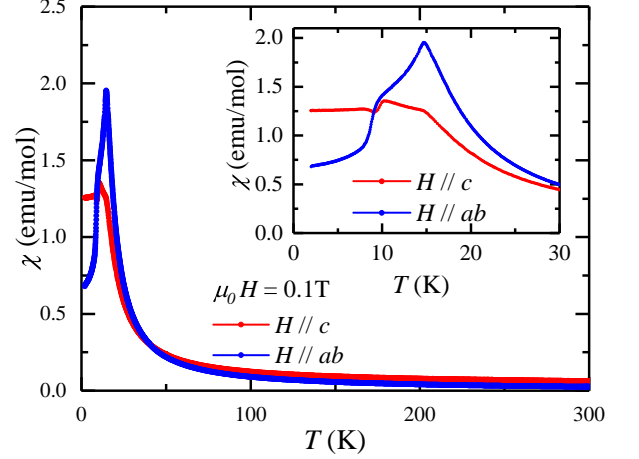


FIG. 2. (Color online) Temperature dependence of the magnetic susceptibility for EuAg_4As_2 measured at $\mu_0 H = 0.1 \text{ T}$ applied in the ab plane and along the c axis, respectively. The inset of the figure shows an enlarged view of magnetic susceptibility at low temperatures.

where χ_0 and C is the temperature-independent constants, θ is the Curie temperature. The fitting result yields an effective moment $\mu_{eff} = 7.95 \mu_B$, close to the theoretical value of Eu^{2+} moments ($g\sqrt{S(S+1)} = 7.94 \mu_B$, $S = 7/2$ and $g = 2$), implying that $\text{Eu}^{2+} 4f^7$ electrons are localized, and a positive Curie temperature $\theta = 14.1 \text{ K}$, indicating ferromagnetic (FM) interactions in the paramagnetic (PM) regions (see Table I). At low temperatures, $\chi_{ab}(T)$ exhibits a sharp peak at about 15 K (T_{N2}) and a kink at 10 K (T_{N1}), where the transition temperature T_{N1} is a little bit higher than that reported previously¹⁰ due to the smaller field applied in our measurement, as discussed below. The result confirms that the triangle Eu^{2+} spin sublattices undergo a transition from a PM state to an incommensurate sine modulated AFM state (referred to as AFM-II) at T_{N2} and then to an incommensurate, non-collinear AFM state (referred to as AFM-I) at T_{N1} ^{10,11}. The $\chi_c(T)$ has a similar behavior to that in $\chi_{ab}(T)$ at high temperatures, but $\chi_c(T)$ remains almost unchanged and is larger than that of $\chi_{ab}(T)$ below T_{N1} , suggesting that the Eu^{2+} moments almost lie in the ab plane. Besides, it should be noted that the large residual magnetic moment at $T = 2 \text{ K}$ is consistent with the incommensurate, non-collinear AFM ordered state.

Figure 3(a) shows $\chi_{ab}(T)$ measured at several magnetic fields. At $\mu_0 H = 0.1 \text{ T}$, the AFM-II transition occurs at $T_2^{ab} = 15 \text{ K}$ and the AFM-I transition occurs at $T_1^{ab} = 10 \text{ K}$, as discussed above. It can be seen that with increasing field, both T_1^{ab} and T_2^{ab} are noticeably shifted to lower temperatures. Meanwhile, an additional transition is observed at T_3^{ab} under an external field, characterized by a tiny kink in the $\chi_{ab}(T)$ curves. For $0.3 \text{ T} \leq \mu_0 H \leq 0.6 \text{ T}$, we observe a clearly deviation between ZFC and FC curves at low temperatures, which may be due to the MM transitions occurring in this field

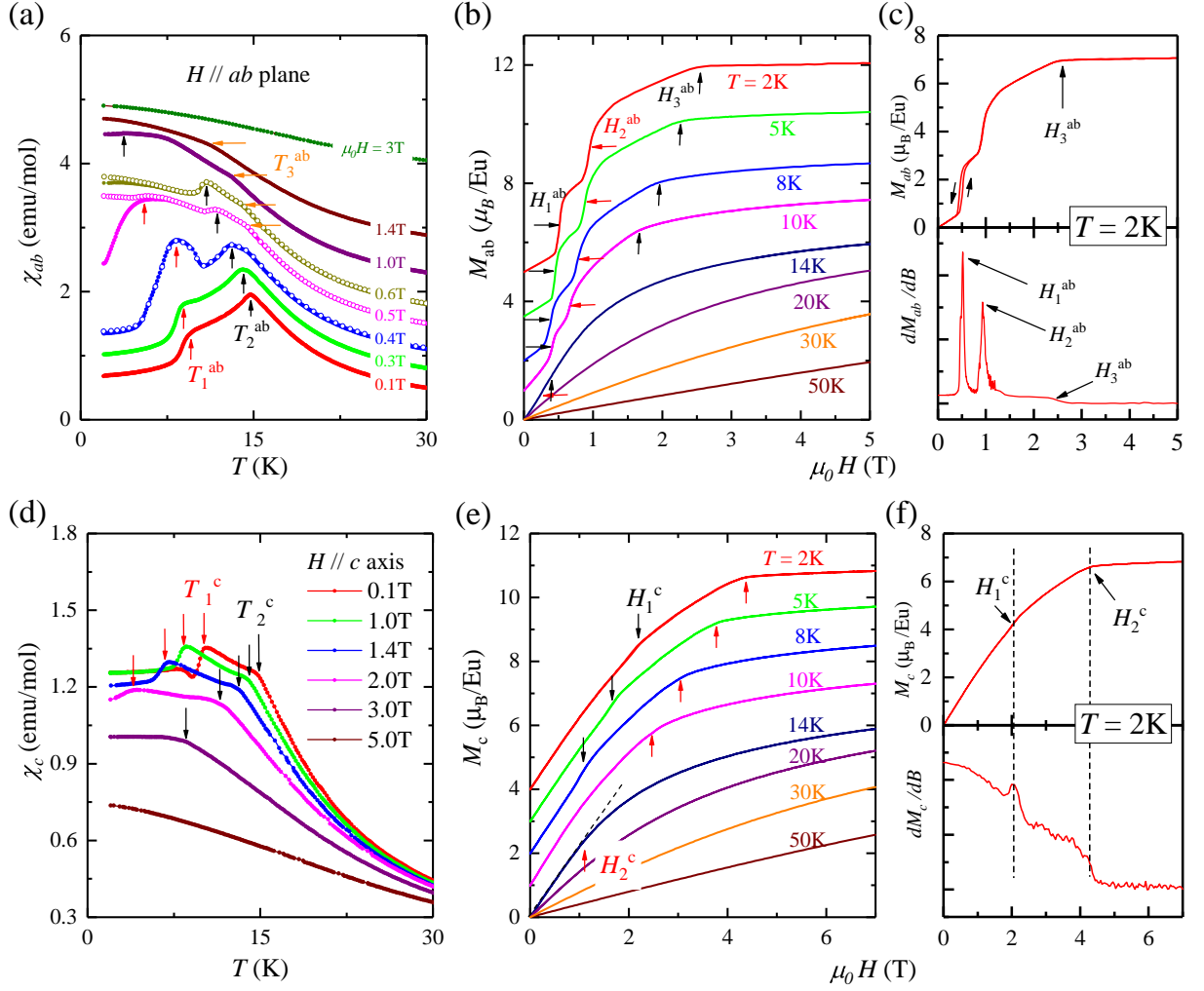


FIG. 3. (Color online) Temperature dependence of magnetic susceptibility of the EuAg₄As₂ single crystal under several selected magnetic fields for $H \parallel ab$ (a) and $H \parallel c$ (d), below $T = 50$ K. For some selected magnetic fields along the ab plane, both field-cooled (FC, hollow circles) and zero-field-cooled (ZFC, solid circles) data are shown. For most other cases, only the ZFC data are shown. In the case of $H \parallel ab$, the data have been shifted for clarity except for the one taken in the field of 0.1 T. Field dependence of magnetization of the EuAg₄As₂ single crystal at various temperatures, with the field parallel to the ab plane (b) and c axis (e). The data taken below $T = 14$ K has been shifted for clarity. (c) The field dependence of M_{ab} (top) and its first derivative (bottom) taken in the field increasing process at $T = 2$ K. (f) The field dependence of M_c (top) and its first derivative (bottom) at $T = 2$ K. The dashed lines are guides to the eyes.

range as discussed below. From the $\chi_c(T)$, it can also be seen that both T_1^c and T_2^c are shifted to lower temperature with increasing magnetic field as shown in Fig. 3(d).

In order to understand these peculiar behaviors of $\chi(T)$, we carried carefully out the isothermal magnetization measurements. Figure 3(b) shows the field dependence of magnetization, $M_{ab}(H)$, for $H \parallel ab$ up to 5 T. At $T = 50$ K, the M_{ab} increases nearly linearly with increasing field, indicating a typical paramagnetic behavior. When $14 \text{ K} \leq T \leq 30 \text{ K}$, the $M_{ab}(H)$ curves exhibit an apparent nonlinear behavior due to the magnetic fluctuation close to the T_{N2} . At $T \leq 10$ K, the $M_{ab}(H)$ exhibits two jumps at H_1^{ab} and H_2^{ab} , respectively, and a

tiny kink at the field H_3^{ab} , indicating three transitions emerging, which will be discussed in details below. With decreasing temperature, the critical field H_2^{ab} shifts to a higher value, while the H_1^{ab} remains almost unchanged. To get more information on the abnormal jumps, we present the M_{ab} data measured at $T = 2$ K in the upper panel of Fig. 3(c). With increasing field, the M_{ab} increases linearly first, which is consistent with the expectation of AFM ground state. Then, it changes sharply at $\mu_0 H_1^{ab} = 0.53 \text{ T} / 0.44 \text{ T}$, when increasing/decreasing magnetic field, respectively, *i.e.*, a hysteresis emerging at this field, corresponding to the first MM transition (MM-I). After the transition, the $M_{ab}(H)$ displays a linear dependence. With the field increasing further, the

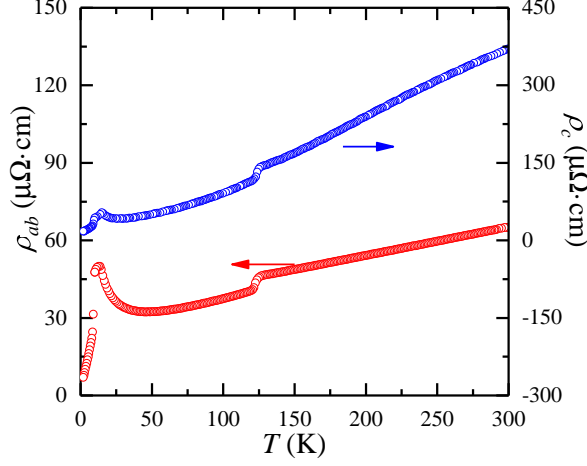


FIG. 4. (Color online) Temperature dependence of the in-plane (left) and out-plane (right) resistivity of EuAg_4As_2 single crystal.

$M_{ab}(H)$ increases again sharply at $\mu_0 H_2^{ab} = 0.95$ T without hysteresis, corresponding to a second MM transition (MM-II), and then turns to display a linear field dependence again. Finally, it saturates to $7.05 \mu_B$ at $\mu_0 H_3^{ab} = 2.53$ T. The critical fields are shown clearer from the derivative plot of $M_{ab}(H)$ as shown in the lower panel of Fig. 3(c). A hysteresis emerges at the MM-I transition, *i.e.*, M_{ab} values measured in the increasing and decreasing field process are not the same, indicating that this transition is the first order. Similar behavior has been reported in the polycrystalline EuAg_4As_2 samples previously, which was explained as a MM transition of the Eu^{2+} moments. However, only one MM transition was observed in this work⁹, different from our results. In addition, we note that the $M_{ab}(H)$ curves for $T > 2$ K still have a small slope in the high field region, which implies a FM-like alignment state rather than a FM ordered state. For comparison, we also measured the isothermal magnetization when the magnetic field is applied in the c axis, as shown in Fig. 3(e), but no MM transition was observed up to 7 T. At $T = 2$ K, the $M_c(H)$ increases slowly with increasing field compared with $M_{ab}(H)$, and displays two kinks around $\mu_0 H_1^c = 2.06$ T, and $\mu_0 H_2^c = 4.14$ T, respectively. A small slope is also observed in the high field region for $M_c(H)$, which doesn't saturate until the highest measured field. At $T_{N1} = 10$ K, the kink in $M_c(H)$ disappears, which may be related to the difference between AFM-I to AFM-II.

Next, we discuss the two MM transitions observed in $M_{ab}(H)$ curves. According to the neutron diffraction result reported in Ref.¹⁰, below T_{N1} , EuAg_4As_2 is an incommensurate antiferromagnet (AFM-I), *i.e.*, the spins of Eu^{2+} rotate around the c axis with a helical arrangement, and around the b axis with a cycloidal arrangement, having a small propagation vector of $\vec{K}_m = (0, 0.1, 0.12)$. Such a complex non-collinear magnetic structure was considered to be resulted from the RKKY in-

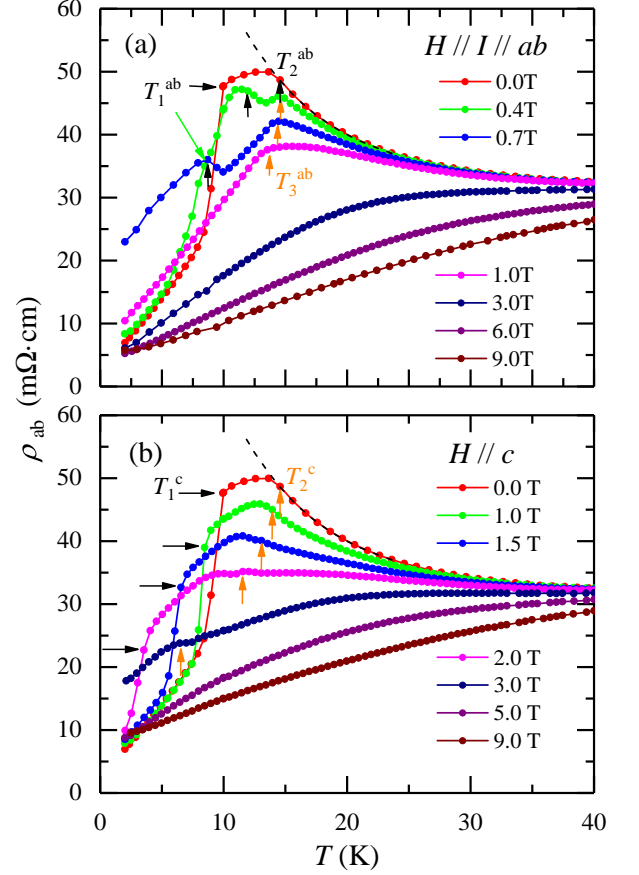


FIG. 5. (Color online) Temperature dependence of in-plane resistivity ρ_{ab} of EuAg_4As_2 single crystal under several selected fields for $H \parallel ab$ (a) and $H \parallel c$ (b), below $T = 40$ K. The dashed lines are guides to the eyes.

teraction in EuAg_4As_2 ¹⁰. As discussed above, with increasing field applied in the ab plane, the M_{ab} undergoes two steep jumps at H_1^{ab} and H_2^{ab} , respectively, the first jump exhibiting a notable hysteresis, while the second one without a hysteresis, then saturates finally to $7.05 \mu_B$ at H_3^{ab} . However, no MM transition was observed as H was applied in the c axis. These results indicated that the spin-alignment of EuAg_4As_2 for $H \parallel ab$ may transit into two metastable states (MSS-I and MSS-II) successively with increasing field. Although the exact arrangement of spins in these metastable states can't be described only by our static magnetization measurements, and is needed to be determined by the neutron diffraction experiments in the future, the corresponding MM transitions are different from that due to the spin-flop (in which the spins are driven perpendicular to the applied magnetic field), which were usually observed in an uniaxial antiferromagnet with low anisotropy, such as in CaCo_2As_2 ¹³. In EuAg_4As_2 , the spin-alignment may have four states, AFM-I (discussed above), MSS-I ($H_1^{ab} < H < H_2^{ab}$), MSS-II ($H_2^{ab} < H < H_3^{ab}$), and FM-like alignment ($H > H_3^{ab}$) under applied magnetic field in the ab plane. Finally, the balance between Zeeman en-

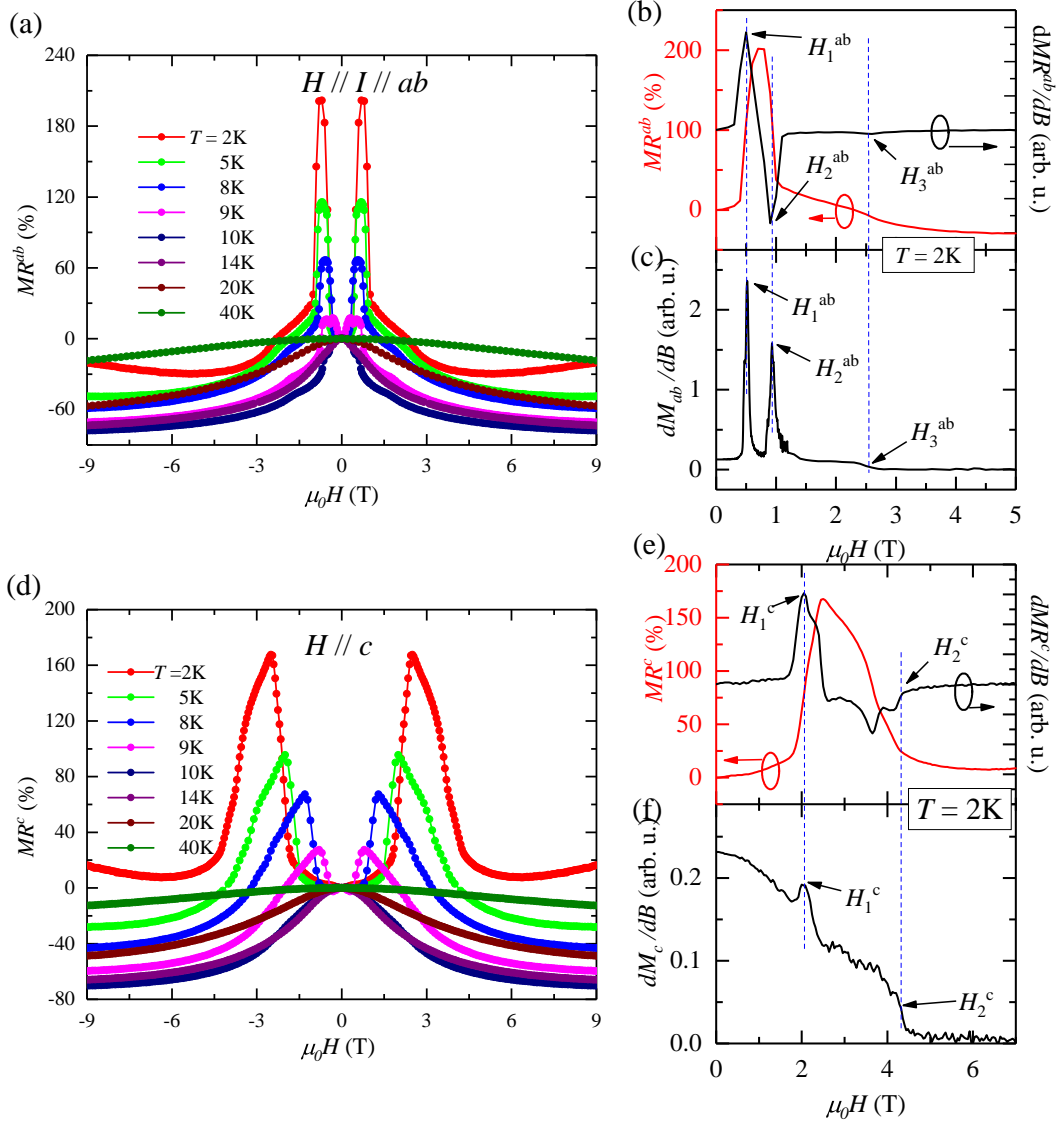


FIG. 6. (Color online) Field dependence of the MR at several temperatures for $H \parallel ab$ (a) and $H \parallel c$ (d). The applied current is parallel to the field in the case of $H \parallel ab$. (b) The field dependence of MR^{ab} (left) and its first derivative (right) at $T = 2$ K. (c) The first derivative of the M_{ab} as a function of field at $T = 2$ K. (e) The field dependence of MR^c (left) and its first derivative (right) at $T = 2$ K. (f) The first derivative of the M_c as a function of field at $T = 2$ K. The dashed lines are guides to the eyes.

ergy, magnetic coupling energy, and magneto-crystalline anisotropy energy lead to that the moments are rotated to the direction of H (in the ab plane). Similar phenomena can also be found in the other rare-earth intermetallic compounds^{14–17}.

Figure 4 shows the electrical resistivity in the ab -plane, $\rho_{ab}(T)$, and along c axis, $\rho_c(T)$, as a function of temperature for a EuAg₄As₂ crystal. The ρ_{ab} and ρ_c at room temperature (300 K) are of $65 \mu\Omega \text{ cm}$ and $370 \mu\Omega \text{ cm}$, respectively, thus the resistivity anisotropy $\rho_c/\rho_{ab} = 5.7$, which is not so large for this layered compound. With decreasing temperature from 300 K, the ρ_{ab} decreases monotonically at first, then drops sharply near $T_s = 120$ K due

to a structural transition¹⁰, and goes through a hump around 15 K, which can be ascribed to the magnetic transitions. The $\rho_c(T)$ exhibits a similar behavior.

Then, we discuss the magnetic responses of $\rho_{ab}(T)$ measured at low temperatures (≤ 40 K) with applied $H \parallel ab$ plane and $H \parallel c$ axis, respectively. Under zero field, the $\rho_{ab}(T)$ exhibits a hump feature starting at $T_{N2} = 15$ K, and a rapid drop around $T_{N1} = 10$ K, which is consistent with the magnetic transitions. For both $H \parallel ab$ and $H \parallel c$, the two transitions shifts to lower temperatures with increasing field, and the resistivity hump is suppressed, resulting in a large MR. Meanwhile, an additional transition is observed at T_3^{ab} in the

case of $H \parallel ab$, characterized by a peak (or kink) in the $\rho_{ab}(T)$ curves, consistent with the $\chi_{ab}(T)$ data as discussed above. In the highest measured field of 9 T, the $\rho_{ab}(T)$ decreases monotonically with decreasing temperature, and no phase transition is observed for both $H \parallel ab$ and $H \parallel c$.

Figure 6(a) shows the field dependence of MR for $H \parallel ab$ measured at several temperatures. In order to eliminate the hysteresis effect in the first MM transition region, all the data are collected in a field increasing process. At $T = 2$ K, the MR^{ab} , defined as $\frac{\rho_{ab}(H, T) - \rho_{ab}(0, T)}{\rho_{ab}(0, T)}$, increases slowly with increasing field at first, then displays a quick rise around $\mu_0 H_1^{ab} = 0.5$ T, and reaches a maximum value of 202% at 0.7 T, then decreases rapidly until $\mu_0 H = 1$ T, exhibiting a peak-like feature. With increasing field further, the MR^{ab} decreases gradually to negative values, reaches a minimum, then increases a little, consistent with the behavior of the FM-like state. The critical fields at $T = 2$ K are clearly shown in the first derivative of MR^{ab} , and are also consistent with that of dM_{ab}/dH [see Fig. 6(b) and 6(c)], indicating that the spin-alignment of MSS-I has the strongest scatter to electrons, resulting in a large positive MR. With increasing temperature, the positive MR^{ab} at low fields is significantly suppressed, and disappears for $T \geq 10$ K. Instead, a large negative MR^{ab} emerges for $T > 10$ K in the whole measuring field range, which is probably contributed to the reduction of spin disorder scattering. At $T = 10$ K, the MR^{ab} can even reach -78% at 9 T. With increasing temperature further, the magnitude of the negative MR^{ab} decreases, exhibiting a maximum at T_{N1} . This behavior is similar to that observed in the well-known perovskites-based manganites (CMR systems)¹⁸. It is interesting that the negative MR^{ab} is also observed at higher temperatures far above T_{N2} in EuAg_4As_2 , such as, the MR^{ab} reaches as large as -21% at 9 T for $T = 40$ K, as shown in Fig. 6(a), which usually occurs in the ferromagnetically ordered state. We also note that there is a sign crossover around 65 K, beyond which MR^{ab} is a negligibly small, but positive value (not shown here). So we suggest that the large negative MR above T_{N2} may origin from the precursor effect of $\text{Eu}^{2+} 4f^7$ moment long-range magnetic ordering, as discussed in Eu_2CuSi_3 and $\text{Eu}_3\text{Ni}_4\text{Ga}_4$ ^{4,14}.

As shown in Fig. 6(d), the field dependence of MR^c ($H \parallel c$) is quite similar to the behavior in $MR^{ab}(H)$. At $T = 2$ K, with increasing field, the MR^c increases gradually at first, then increases sharply at $\mu_0 H_1^c = 2.1$ T, goes through a maximum (over 160% at 2 K and 2.5 T), and decreases steeply until $\mu_0 H_2^c = 4.1$ T, reaches a minimum, finally increases a little until the highest measuring field (9 T). The MR^c behavior is consistent with that of $M_c(H)$, as shown in Fig. 6(f). Compared with dM_c/dB , several additional peaks were observed in the first derivative of MR^c , which may be ascribed to the movement of magnetic domain walls with the external field. These results imply that when the magnetic field is applied along the c axis, the spin alignment in AFM-II

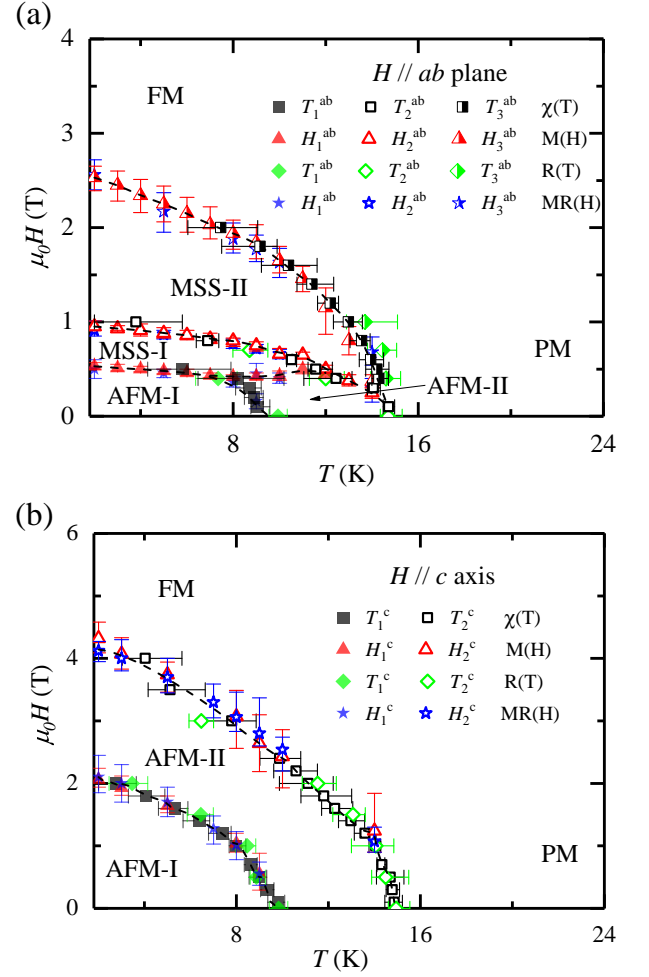


FIG. 7. Magnetic phase diagram of EuAg_4As_2 for $H \parallel ab$ plane (a) and $H \parallel c$ axis (b). The symbols are extracted from M - T (black), M - H (red), R - T (green) and MR - H (blue) curves, respectively. The dashed lines are guides to the eyes.

has the strongest scatter to electrons flowing in the ab plane (corresponding to ρ_{ab}), resulting in a large positive MR. With increasing temperature, the H_1^c and H_2^c , and the positive MR decrease. At $T = 10$ K, the peak of positive MR disappears, and the largest negative MR (up to -70% at 9 T) emerges. Up to 40 K, far above T_{N2} , a large negative MR remains (-20%, 9 T). Another, except for 2 K, the MR decreases monotonically with increasing magnetic field after the positive peak at all temperatures, which maybe related the spin dynamics.

As discussed above, such complicated behaviors exhibiting in $\rho_{ab}(T)$ and $\rho_c(T)$ in EuAg_4As_2 crystal are related to the magnetic ground states at different magnetic fields (H) and various temperatures (T). In order to clarify the relationship between the transport and magnetic order, we construct the $H(T)$ phase diagram based on the resistivity and magnetization data measured at various (H , T), as shown in Fig. 7(a) ($H \parallel ab$) and Fig. 7(b) ($H \parallel c$), respectively. For $H \parallel ab$ plane, the phase

diagram can be divided into six regions, AFM-I, AFM-II, PM, FM-like alignment region, and two metastable states (MSS-I and MSS-II). At $T = 2$ K, the compound undergoes two MM transitions from AFM-I with increasing field and enters finally the FM-like alignment region, with the critical field of 0.5 T, 0.95 T and 2.5 T, respectively. It should be noted that the boundary between FM-like alignment region and PM state can't be precisely determined. For $H \parallel c$ axis, the phase diagram can be divided into four regions, AFM-I, AFM-II, PM and FM-like alignment region, two phase boundaries are clearly distinguished. At $T = 2$ K, EuAg_4As_2 crystal undergoes magnetic phase transitions from the AFM-I phase to the intermediate AFM-II phase, then to the FM-like alignment region with increasing magnetic field, with the critical field of 2.1 T, and 4.2 T, respectively. Another, as shown in Fig. 7(a) and Fig. 7(b), the phase boundaries deduced from the data of magnetization and resistivity measurements, respectively, are well consistent with each other, indicating that the complicated magnetotransport properties are related to the magnetic orders, especially the large positive MR occurring in a narrow magnetic range provides a chance for application on magnetic sensors.

In summary, we studied systematically the magnetic and transport properties of EuAg_4As_2 single crystals by using magnetization and resistivity measurements. Under zero field, it was confirmed that two magnetic transitions occur at $T_{N1} = 10$ K and $T_{N2} = 15$ K, respectively, with the magnetic moments almost lying in the ab plane. With increasing field, the two magnetic transitions are

driven noticeably to lower temperatures, indicating that they are tunable ground states. At $T = 2$ K, two successive MM transitions were observed at 0.5 T and 0.95 T, respectively, when applying magnetic field in the ab plane. On the other hand, no MM transition was detected below 7 T for $H \parallel c$. For both $H \parallel ab$ and $H \parallel c$, an anomalous field dependence of MR was observed, which shows a positive, unexpected large value at low fields below 10 K, and a large negative value at high fields/intermediate temperatures, indicating a rather disordered spin-alignment state in the intermediate phases. Such anomalous field dependence of MR is rather rare, and may have potential application in the future magnetic sensors. Interestingly, large negative MR is seen even at 40 K, which is far above the magnetic transition temperature. According to these results, we established the phase diagrams of EuAg_4As_2 for both $H \parallel ab$ and $H \parallel c$.

IV. ACKNOWLEDGEMENTS

This research is supported by the Ministry of Science and Technology of China under Grants No. 2016YFA0300402 and No. 2015CB921004 and the National Natural Science Foundation of China (NSFC) (No. 11974095, 11374261), the Zhejiang Natural Science Foundation (No. LY16A040012) and the Fundamental Research Funds for the Central Universities.

* These authors contributed equally to this work.

[†] hdwang@hznu.edu.cn

[‡] mhfang@zju.edu.cn

¹ A. Mitsuda, H. Wada, M. Shiga, H. Aruga Katori, and T. Goto, *Phys. Rev. B* **55**, 12474 (1997).

² C. Feng, Z. Ren, S. Xu, S. Jiang, Z. Xu, G. Cao, I. Nowik, I. Felner, K. Matsubayashi, and Y. Uwatoko, *Phys. Rev. B* **82**, 094426 (2010).

³ H. Masuda, H. Sakai, M. Tokunaga, Y. Yamasaki, A. Miyake, J. Shiogai, S. Nakamura, S. Awaji, A. Tsukazaki, H. Nakao, Y. Murakami, T.-h. Arima, Y. Tokura, and S. Ishiwata, *Sci. Adv.* **2**, e1501117 (2016).

⁴ S. Majumdar, R. Mallik, E. V. Sampathkumaran, K. Rupprecht, and G. Wortmann, *Phys. Rev. B* **60**, 6770 (1999).

⁵ C. Yi, S. Yang, M. Yang, L. Wang, Y. Matsushita, S. Miao, Y. Jiao, J. Cheng, Y. Li, K. Yamaura, Y. Shi, and J. Luo, *Phys. Rev. B* **96**, 205103 (2017).

⁶ D. Gignoux and D. Schmitt, *J. Magn. Magn. Mater.* **100**, 99 (1991).

⁷ S. S. Stoyko, M. Khatun, C. S. Mullen, and A. Mar, *J. Solid State Chem.* **192**, 325 (2012).

⁸ B. Shen, E. Emmanouilidou, X. Deng, A. McCollam, J. Xing, G. Kotliar, A. I. Coldea, and N. Ni, *Phys. Rev.*

B **98**, 235130 (2018).

⁹ B. Gerke, C. Schwickert, S. S. Stoyko, M. Khatun, A. Mar, and R. Poettgen, *Solid State Sci.* **20**, 65 (2013).

¹⁰ B. Shen, C. Hu, H. Cao, X. Gui, E. Emmanouilidou, W. Xie, and N. Ni, arXiv:1809.07317 [cond-mat.str-el].

¹¹ D. H. Ryan, S. L. Bud'ko, C. Hu, and N. N., *AIP Adv.* **9**, 125050 (2019).

¹² S. L. Bud'ko, L. Xiang, C. Hu, B. Shen, N. Ni, and P. C. Canfield, *Phys. Rev. B* **101**, 195112 (2020).

¹³ B. Cheng, B. F. Hu, R. H. Yuan, T. Dong, A. F. Fang, Z. G. Chen, G. Xu, Y. G. Shi, P. Zheng, J. L. Luo, and N. L. Wang, *Phys. Rev. B* **85**, 144426 (2012).

¹⁴ Anupam, C. Geibel, and Z. Hossain, *J. Phys.: Condens. Matter* **24**, 326002 (2012).

¹⁵ J. Tong, J. Parry, Q. Tao, G.-H. Cao, Z.-A. Xu, and H. Zeng, *J. Alloys Compd.* **602**, 26 (2014).

¹⁶ S. Jiang, Y. Luo, Z. Ren, Z. Zhu, C. Wang, X. Xu, Q. Tao, G. Cao, and Z. Xu, *New J. Phys.* **11**, 025007 (2009).

¹⁷ F. Weber, A. Cosceev, S. Drobnik, A. Faißt, K. Grube, A. Nateprov, C. Pfleiderer, M. Uhlarz, and H. v. Löhneysen, *Phys. Rev. B* **73**, 014427 (2006).

¹⁸ R. von Helmolt, J. Wecker, B. Holzapfel, L. Schultz, and K. Samwer, *Phys. Rev. Lett.* **71**, 2331 (1993).